THE JOURNAL OF PHYSICAL CHEMISTRY Letters

Letter

pubs.acs.org/JPCL

Interfacial Modification of Perovskite Solar Cells Using an Ultrathin MAI Layer Leads to Enhanced Energy Level Alignment, Efficiencies, and Reproducibility

Zafer Hawash,[†] Sonia R. Raga,[†] Dae-Yong Son,[‡] Luis K. Ono,[†] Nam-Gyu Park,*[,‡] and Yabing Qi*[,†]

[†]Energy Materials and Surface Sciences Unit (EMSS), Okinawa Institute of Science and Technology Graduate University (OIST), 1919-1 Tancha, Onna-son, Okinawa 904-0495, Japan

[‡]School of Chemical Engineering and Department of Energy Science, Sungkyunkwan University (SKKU), Suwon 440-746, Korea

Supporting Information

ABSTRACT: For the first time, we intentionally deposit an ultrathin layer of excess methylammonium iodide (MAI) on top of a methylammonium lead iodide (MAPI) perovskite film. Using photoelectron spectroscopy, we investigate the role of excess MAI at the interface between perovskite and spiro-MeOTAD hole-transport layer in standard structure perovskite solar cells (PSCs). We found that interfacial, favorable, energy-level tuning of the MAPI film can be achieved by controlling the amount of excess MAI on top of the MAPI film. Our XPS results reveal that MAI dissociates at low thicknesses (<16 nm) when deposited on $MAPbI_3$. It is not the MAI layer but the dissociated species that leads to the interfacial energy-level tuning. Optimized interface energetics were verified by solar cell device testing, leading to both an increase of 19% in average steady-state power conversion efficiency (PCE) and significantly improved reproducibility, which is represented by a much lower PCE standard deviation (from 15 ± 2% to 17.2 ± 0.4%).

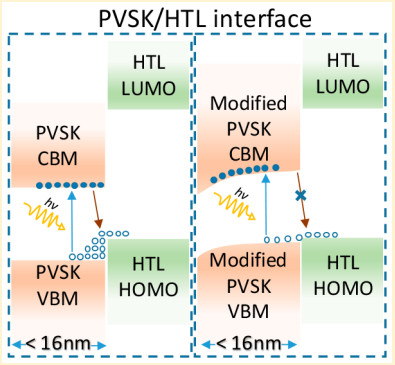

INTRODUCTION

The emergence of organic and inorganic hybrid perovskite (PVSK) semiconductors has captured the attention of materials scientists with its promising applications in electronic and optoelectronic devices.[1] PVSK semiconductors are currently being intensively investigated for applications such as light-emitting diodes,[2−4] lasing,[5,6] energy storage,[7] water splitting,[8,9] photodetectors,[10] and memory devices.[11] In particular, outstanding progress has been achieved in photovoltaic (PV) applications employing PVSK materials.[12,13] Since the first solid-state PVSK solar cells reported by Park and coauthors in 2012, outstanding progress has been achieved in PV applications employing PVSK materials.[14] To date, PVSK solar cells (PSCs) have achieved impressive power conversion efficiencies (PCEs) exceeding 22%.[15] Despite these impressive PCEs, there is still a great need to understand the fundamental chemical and energetic properties of PVSK materials in device structures, which require rational fabrication strategies to yield efficient and stable optoelectronic devices.

To achieve better power conversion efficiencies, it is necessary to minimize recombination and to maximize carrier extraction efficiency at interfaces between different layers in a solar cell. One of the critical steps to achieve this goal is to optimize energy level alignment at the interfaces.[16] Optimal energy level alignment relies on fine adjustment of the energy levels of selective contacts to match the energy levels of the PVSK material and vice versa.

Methylammonium lead iodide (MAPI) PVSK is a widely employed PVSK material and solar cells based on MAPI exhibit high PCEs. MAPI films show n-type behavior when deposited on insulating or n-type substrates.[17,18] In standard perovskite solar cell (PSC) structure, for example, with FTO/TiO_2 as electron-selective contact, the conduction band (CB) of the electron transport layer (ETL) has a desirable alignment with the CB of PVSK.[18−20] On the contrary, an interfacial increase in the valence band (VB) leading edge of the PVSK layer would provide better hole extraction and minimized carrier recombination at the interface between PVSK and the spiro-MeOTAD hole-transport layer (HTL). Therefore, fine control of the MAPI PVSK interface with the HTL is crucial to achieve optimal energy level alignment and thus maximize charge extraction efficiency and PCE.

The CB of MAPI is often reported to be almost pinned to the Fermi level in standard-structure PSCs.[18−21] As pointed out by Olthof,[21] the interpretation of the n-type behavior in MAPI generally shown by ultraviolet photoelectron spectroscopy (UPS) is complex, and several factors such as (i) surface stoichiometry, (ii) the type of defects present, (iii) influence from the underneath substrate, and others may lead to such an observation. Deficient amounts of methylammonium iodide (MAI) in the precursor solution of MAPI or short annealing

Received: June 14, 2017
Accepted: August 2, 2017
Published: August 2, 2017

DOI: 10.1021/acs.jpclett.7b01508
J. Phys. Chem. Lett. 2017, 8, 3947−3953

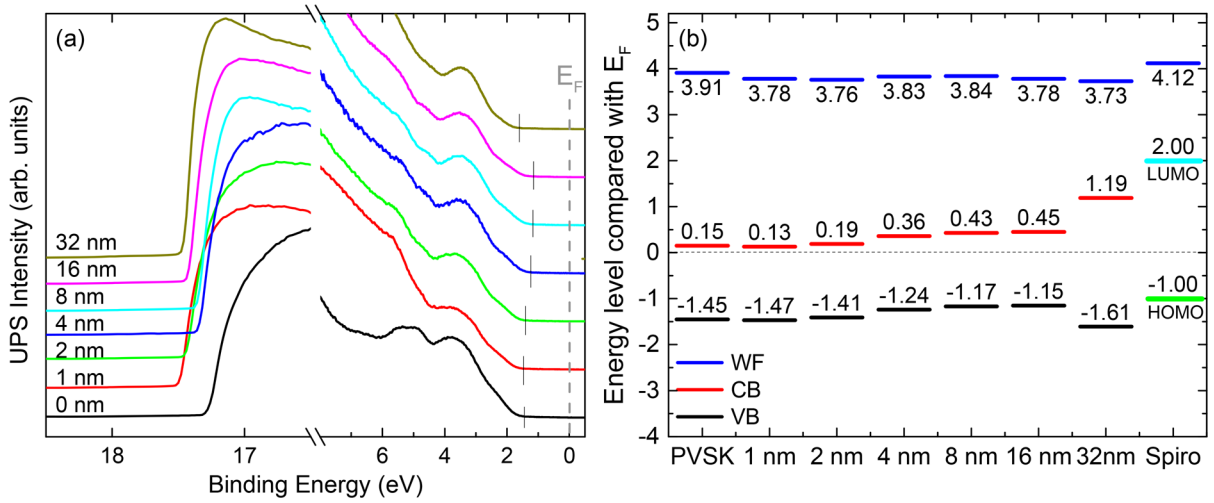

Figure 1. (a) UPS spectra (He−Iα = 21.22 eV) corresponding to valence band (VB) and cutoff regions of the pristine perovskite (PVSK) sample and the samples with an additional layer of excess MAI of various thicknesses. (b) Schematic energy diagram of VB, conduction band (CB), and work function (WF) with respect to Fermi energy (E_F) corresponding to the pristine PVSK sample, afterward modification by MAI evaporation, and spiro-MeOTAD (spiro). A schematic energy diagram with respect to vacuum energy level (E_V) can be found in the Supporting Information. CB values are derived based on the optical band gap of MAPI PVSK and VB, and, in the case of a 32 nm MAI layer, the MAI band gap is used.

times were also reported to lead to an n-type behavior of the MAPI PVSK film.[22] UPS and XPS measurements show that energy levels of MAPI PVSK can be tuned up to 1 eV, depending upon the preparation methods.[23] It was shown using inverted structure with 2-step PVSK film preparation method that the doping density of the PVSK film is highly dependent on the length of the MAI loading period of time. Short length of MAI loading time resulted in low PCEs, which substantially increased with length up to 1 min. Longer time resulted in dramatic decrease in the PCEs and was attributed to excess of uncoordinated ions.[24] High PCEs and reproducibility were also achieved with one-step method with a small amount of excess MAI in the precursor solution. The higher PCEs and reproducibility were attributed to MAI layer formation at the grain boundaries of the PVSK film. The passivated grain boundaries are believed to suppress nonradiative recombination and enhance charge-carrier extraction.[25]

On the contrary, it was proposed that excess MAI might remain on the PVSK surface and therefore reduce the surface conductivity.[26] Interestingly, excess PbI_2 incorporation in the precursor solution was also reported to improve the PCEs and was suggested to improve the crystallinity of the perovskite film.[27] Excess PbI_2 in the precursor solution was also discussed as a "double-edge sword", leading to higher PCEs for PbI_2-rich cells and higher open-circuit voltage (V_{oc}) for MAI-rich cells.[28] However, the exact influence of excess MAI or where it should be located in PSCs has remained conjectural.

In this work, we introduce an ultrathin MAI layer by vacuum evaporation to simulate and study the effects of various amounts of excess MAI at the interface between the MAPI PVSK layer and the spiro-MeOTAD HTL. Our XPS and UPS measurements suggest that the additional ultrathin MAI layer deposition leads to efficient interfacial energy-level tuning of the MAPI PVSK films. By systematically examining energy level evolution at the interface as a function of MAI layer thickness, an excess MAI thickness of 8 nm corresponded to the optimal interfacial energy level alignment with spiro-MeOTAD (spiro). Furthermore, we verify the validity of such an optimal condition with PSC testing. Samples were prepared using standard PSC structure consisting of FTO/TiO_2 compact layer/TiO_2 mesoporous layer/MAPI/spiro. The PVSK layer was prepared using one-step solution processing with diethyl ether (DEE) antisolvent.[29,30] One sample, which served as the reference sample, was prepared without any modification of the PVSK layer, while each of the remaining samples was prepared with an additional ultrathin layer of MAI on top of the PVSK layer by thermal evaporation under vacuum. Nominal thicknesses of the evaporated MAI ultrathin films were 1, 2, 4, 8, 16, and 32 nm. The nominal thickness values were measured with a calibrated quartz crystal microbalance (QCM) inside the MAI evaporation chamber. The fabricated PSCs with optimal interfacial modification show an average steady-state PCE of 17.2%, which is 19% higher than that of reference cells (15%). In addition, device steady-state PCE shows smaller spreading with a PCE standard deviation (σ) of 0.4% as compared with 2% for reference cells, suggesting significantly improved device reproducibility.

Analysis of UPS results for a pristine MAPI PVSK film provide a VB leading edge position of −1.45 eV with respect to the Fermi energy (E_F) (Figure 1), which corresponds to an ionization energy (IE) of 5.36 eV (Figure S1). The addition of small amounts of MAI on top of the PVSK layer resulted in a gradual upshift of the VB from −1.45 to −1.15 eV, which resembles p-doping behavior.[22] The distance between E_F and the VB was reduced by 0.3 eV (pristine vs 16 nm). On the contrary, no drastic changes in WFs were noticed as a function of MAI layer thickness (Figure 1b). As shown in Figure S1, gradual and systematic decrease in IE is observed as the additional MAI layer is increased.[23,31] The IE changes relate to the chemical composition changes on the perovskite surfaces, which is discussed later when discussing the XPS results. For example, the IE of the PVSK layer with an additional 16 nm MAI layer was 4.93 eV, as compared with 5.36 eV in the case of pristine PVSK films (Figure S1). Therefore, the energy shift in the BEs of the VB versus E_F and IE versus vacuum level (E_V) (Figure 1a) is different (0.3 vs 0.43 eV), which suggests that this is not a doping effect in the strict sense. A doping effect would be expected to induce a rigid shift of the whole UPS

DOI: 10.1021/acs.jpclett.7b01508
J. Phys. Chem. Lett. 2017, 8, 3947−3953

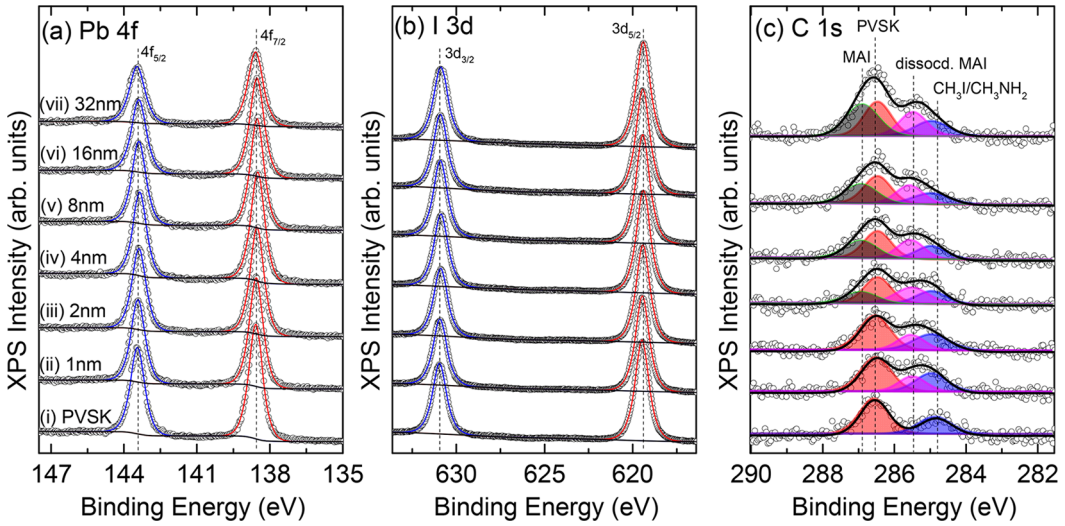

Figure 2. XPS spectra (Al−Kα = 1486.6 eV) corresponding to (a) Pb-4f, (b) I-3d, and (c) C-1s core levels of the pristine PVSK film (i) and the samples after depositing an additional excess MAI layer of 1 (ii), 2 (iii), 4 (iv), 8 (v), 16 (vi), and 32 nm (vii).

spectrum toward E_F (Figure 1a). The observed energy shift suggests a nonstoichiometric nature of the deposited MAI layer on top of the perovskite film. The nonstoichiometric nature that is expected here suggests that the MAI molecules break, which will be discussed in more detail based on the XPS results. Additional evaporation of MAI with nominal values greater than 16 nm resulted in an opposite effect. For example, the evaporation of 32 nm of MAI resulted in ∼0.4 eV shift away from E_F to −1.61 eV with a corresponding IE of 5.34 eV. The schematic energy diagrams with respect to the E_V extracted from UPS data can be found in the Supporting Information (Figure S1).

After UPS measurements, XPS (Al−Kα = 1486.6 eV) was performed on the samples to monitor the chemical states changes and evolution. Figure 2 shows the XPS core levels of Pb-4f (a), I-3d (b), and C-1s (c) of the PVSK films with different MAI nominal thicknesses. Interestingly, there were no detectable shifts in the binding energies (BEs) of the core level of Pb-4f (Figure 2a). The Pb-4f$_{7/2}$ peak maximum for the pristine PVSK film was found at a BE of 138.58 eV and showed almost no shift, even after evaporation of a 32 nm MAI layer (∼0.01 eV). The Pb-4f signal is still detected with a 32 nm layer of MAI, indicating an interfacial modification rather than a thick conformal layer formation of MAI on top of the PVSK film. In addition, we have prepared a sample with 120 nm of MAI on PVSK to examine the possibility of having a conformal layer with excessive amount of MAI (Figure S2). However, the Pb-4f signal was still detected. Therefore, the interaction chemistry between MAI and MAPI needs be considered instead of a simple physical deposition of an inert MAI conformal layer on MAPI. Possible scenarios include (i) MAI or dissociated species may penetrate into the MAPI film and (ii) the dissociated species from MAI are volatile species and may leave the MAPI surface leading to a detectable level of Pb-4f signal by XPS. Here we focus on the Pb-4f peaks because Pb is the only element that we can correlate directly with the underlying layer of MAPI PVSK because all other elements are also present in MAI. XPS has a deeper probing depth compared with UPS (because of a longer mean escape depth for photoelectrons with higher kinetic energy).[32] We observed almost no shift in the BEs of Pb-4f core levels. Therefore, it is clear that the observed VB edge shift is taking place at the very interface at no more than 2 nm depth, which is the expected mean escape depth for UPS.

Similarly, no shifts were observed in the BEs of the core levels of I-3d (Figure 2b). The I-3d$_{5/2}$ peak maximum for the pristine sample was found at a BE of 619.47 eV, and the maximum observed change in BE (0.07 eV) was within measurement uncertainty. Similarly, N-1s core level spectra did not show any shift in the BEs of the peak maximum (Figure S3a). The oxygen core level was also monitored for all samples, and the detected amount was <1% (Figure S3b).

In the case of the C-1s core-level spectrum (Figure 2c), nonmodified PVSK films showed two main peaks with maxima located at BEs of 286.54 and 284.83 eV, respectively. The C-1s peak at a higher BE of 286.54 eV is reported to be associated with carbon in crystalline PVSK films. The origin of the C-1s peak at a lower BE of 284.83 eV remains controversial at present, and, currently, it has been proposed that this peak could originate from C in CH_3I[33] or in CH_3NH_2[34] or remaining solvents.[18,31,35,36] After depositing a 1 nm MAI layer, a new peak located between the aforementioned two peaks at a BE of 285.46 eV was observed. In the current stage, we tentatively assign this peak to dissociated MAI species (dissocd. MAI). As more MAI is deposited, another new peak appeared in the C-1s region with the peak maximum at a BE of 286.86, the intensity of which gradually increased as MAI film thickness increased. Simultaneously, a behavior of MAI electronic properties was observed with UPS, which could be due to the progressive formation of a pure MAI layer on top of the PVSK film. An alternative explanation will be provided based on the changes in the atomic ratios discussed below.

Atomic concentration variations of all measured core levels (Figure S4a,b) showed that pristine PVSK films have Pb:I:C(PVSK):N ratio of 1.0:2.9:1.1:1.1, which is in good agreement with MAPI PVSK that shows ideal ratios of 1:3:1:1. However, our best performing solar cells (4 nm excess MAI deposition) showed nonstoichiometric ratios of 1.0:3.0:1.6:1.1 (Pb:I:C(PVSK):N), indicating that the MAI modification effect is *not* an extra conversion step of the nonconverted PbI_2 layer on the surface to PVSK. Therefore, the excessive carbon observed here is believed to be from dissociated MAI species. The nitrogen signal did not increase, possibly due to release of ammonia gas[37] or other nitrogen-containing gas species.

DOI: 10.1021/acs.jpclett.7b01508
J. Phys. Chem. Lett. 2017, 8, 3947−3953

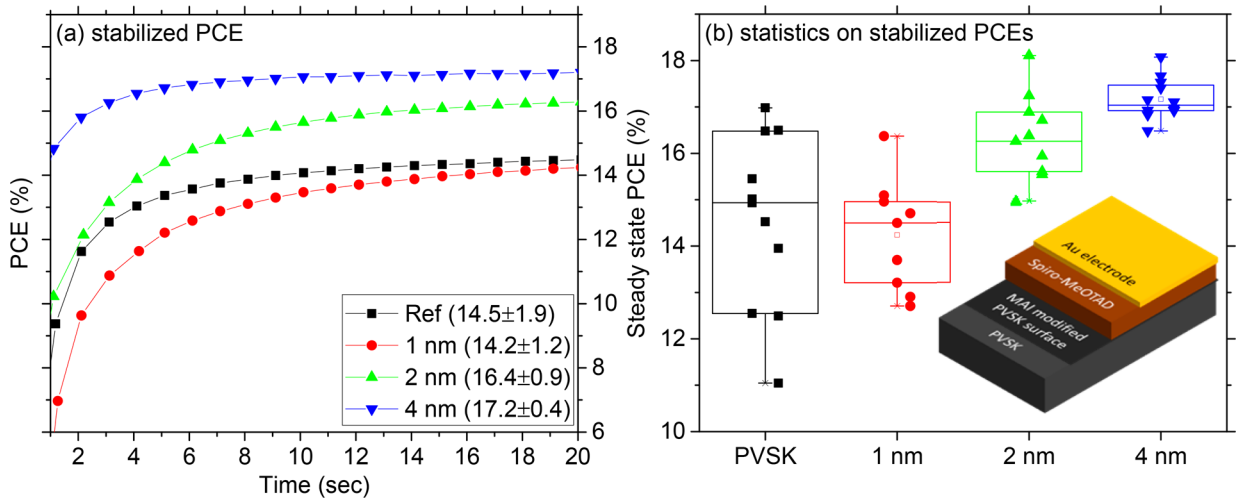

Figure 3. (a) Average steady-state PCE from all measured devices and (b) statistics on steady-state PCE for PVSK solar cells as a function of excess MAI layer thickness. The inset shows a schematic of the interface modification.

Detailed plots illustrating atomic ratio variations of iodine, carbon, nitrogen, and all different types of carbon species for all samples can be found in Figure S4.

After deposition of 32 nm MAI, the atomic concentration of N-1s and I-3d increased substantially while the concentration of C-1s from PVSK in the total C-1s concentration decreased (Figure S4). Further surface chemistry was studied by X-ray diffraction (XRD) (Figure S5). The characteristic MAI peaks are not observed, providing strong evidence that MAI dissociates, as corroborated by our XPS analysis. Instead, additional peaks in the XRD spectra are obtained, in particular, at 11.45 and 24.9°. The origin of these peaks are controversial in the literature. Some reports attribute it to bihydrated perovskite $MA_4PbI_6{\cdot}2H_2O$.[38] The most established consensus is that it originates in the presence of excess MAI, for example, in precursor solution or long dipping time in case of sequential deposition.[39] These reports attribute the 11.45° peak to a low-dimensional layered structure of MA_4PbI_6, where MAI acts as a matrix structure with embedded PbI_2.[40] The nitrogen to iodine ratio changes from the original value of approximately 1:3 (for pristine PVSK) to approximately 1:2 (for the PVSK sample with 32 nm MAI). A ∼0.1 eV increase in the full width at half-maximum (fwhm) of the I-3d spectra of the same sample (with 32 nm MAI) is observed. In an optimal MAI sample, the nitrogen to iodine ratio is 1:1. The combination of three observations (i.e., the N:I ratio changes from the original value of 1:3 for pristine PVSK to a value closer to that in MAI, fwhm increases, and the VB level observed by UPS downshifts) suggests that with this large amount of MAI on top of PVSK the surface is increasingly dominated by the properties of MAI.

UPS and XPS measurements provided explicit evidence that the additional ultrathin MAI layer efficiently tunes the energy level of the PVSK at the interface with the HTL. As can be seen from Figure 1b, a favorable energy level alignment between PVSK and spiro would be achieved if an ultrathin layer of MAI was implemented at the interface. This ultrathin layer would clearly enhance hole extraction due to staircase energy level alignment, which is achieved with the interfacial modification of the PVSK layer.[41,42] Also, recombination at this interface is expected to be reduced due to the decreased number of electrons at the interface as a result of slight band bending at the top of the PVSK/MAI layer. Therefore, following our findings, we fabricated solar cells with MAI modification. The fabricated solar cells used the same structure, as was used for UPS/XPS studies. The only difference was that for devices we deposited a doped spiro layer by spin-coating and a gold electrode by vacuum evaporation on top of pristine/MAI-modified PVSK. After gold evaporation, devices were left overnight in relatively low humidity to achieve better electrical properties and a HOMO level of 1 eV below E_F for spiro (Figure 1b), which provides better energy level alignment with the modified PVSK.[43,44]

Impressive enhancement in steady-state PCE was observed for the cells with an additional 2 and 4 nm films of MAI, which is in good agreement with the improved energy level alignment at the interface between MAI-modified PVSK and spiro HTL. Reference cells showed an average stabilized PCE of 14.5%. In comparison, cells with an additional 4 nm MAI layer showed a significantly improved steady-state PCE up to 17.2% (Figure 3a). In addition, cells with an additional 4 nm MAI layer showed much lower standard deviation (σ) in PCE, indicating better batch-to-batch and sample-to-sample reproducibility (Figure 3b). Cells with an additional 4 nm MAI layer showed σ of 0.4% compared with the reference cells with σ of 1.9%. The improvement in PSC device performance and reproducibility highlights the importance of interfacial modification on PSC device performance. In particular, the low value of σ suggests better reproducibility, consistent with previous reports that showed enhanced reproducibility with excess amounts of MAI in precursor solutions.[25] The improved reproducibility is possibly a benefit of the better-defined PVSK/HTL interface for cells with excess interfacial MAI, as compared with reference cells, in which interface properties (e.g., energetics) may sensitively depend on PVSK film preparation conditions.

In summary, we clarify the role of excess MAI at the interface between PVSK and spiro HTL in standard structure PVSK cells. We simulate the situation by vacuum depositing a layer of excess MAI on top of a PVSK film. Photoelectron spectroscopy results reveal efficient interfacial energy level tuning of PVSK as a function of the excess MAI layer thickness. By systematically examining the energy level at the interface as the MAI layer thickness increased, we identified the optimal interfacial energetic and the corresponding interfacial MAI layer thickness. Our XPS reveals that the initial thin layer of MAI dissociates

DOI: 10.1021/acs.jpclett.7b01508
J. Phys. Chem. Lett. 2017, 8, 3947−3953

when in contact with MAPI. It is not the MAI layer but the dissociated species that leads to the interfacial energy-level tuning. The validity of such an optimal condition was verified with solar cell device testing. Solar cells showed an impressive enhancement in reproducibility and stabilized power conversion efficiencies of 17.2 ± 0.4% (MAI thickness ∼4 nm) as compared with 14.5 ± 1.9% in the case of reference cells. Our findings not only provide vital new insight into the role of excess MAI in PSCs but also indicate the importance of interfacial modification on both performance and reproducibility of PSC devices.

EXPERIMENTAL METHODS

The electronic properties of doped PVSK films were characterized by UPS (Kratos AXIS ULTRA HAS, He−Iα = 21.22 eV). The leading edge of the VB was extracted from logarithmic intensity scale (Figure S6). The analysis of UPS was complemented by XPS (Kratos AXIS ULTRA HAS, monochromated Al−Kα = 1486.6 eV). XPS was performed to monitor the chemical states of the pristine PVSK films and MAI-treated films. The BE for UPS and XPS was calibrated by measuring the Fermi edge (E_F = 0 eV) and Au-4$f_{7/2}$ (84.0 eV) on a clean Au surface. The estimated energy resolutions of UPS and XPS were 0.14 and 0.7 eV, respectively. PVSK sample was used as reference for fitting the first peaks. For the afterward MAI-treated samples, the fwhm of each spectrum was constrained to a change of ±0.1 eV, and, similarly, the peak positions were constrained to a change of ±0.1 eV. When spectral changes were observed, new peaks were added to complete the curve fit. The new fitted peaks were used as reference for the afterward samples. The peak fittings and standard deviation calculations were performed using CasaXPS 2.3.16 software. The stoichiometry analyses in the C 1s region show the largest standard deviation (∼50%) because of multiple components (four peaks) employed to reproduce the XPS raw data. The atomic ratio analyses for the other elements were estimated to have relative errors with respect to the stoichiometry values below 30%. UV- and X-ray-induced sample damage was monitored by taking five consecutive spectra and comparing those spectra. Time acquisition for each scan varied from 20 to 70 s depending on the core level regions. The five scans were averaged to a single spectrum if no changes were observed among them. Special care was taken to minimize the UV and X-ray exposure time when acquiring UPS/XPS on doped spiro films. No X-ray- or UV-induced damage was observed on PVSK films. Our UPS is nonmonochromated; therefore, He I' satellite ($h\nu$ = 23.09 eV) with ∼2% intensity of primary He I ($h\nu$ = 21.22 eV) is expected.[32,45] We numerically corrected the UPS spectra to minimize the effect of satellite peaks that arise as a result of the polychromatic nature of the He I line.[23,32,45]

Solar cell devices were prepared by cleaning the conductive substrates (FTO22−7, OPVTech) using a sequence of brushing with sodium dodecyl sulfate, rinsing with Milli-Q water and sonicating in a 2-propanol bath for 15 min. A ∼70 nm layer of compact TiO_2 was deposited by spraying a solution of Ti (IV) diisopropoxide bis(acetylacetonate) (75%) in isopropanol (Aldrich) on the FTO heated at 480 °C in four rounds of 3 s each spray. After the substrates cooled to room temperature, a TiO_2 mesoporous layer ∼150 nm was deposited by spin-coating a diluted paste (90-T, Dyesol) in 1-butanol 1:5 wt at 4500 rpm for 30 s. The spin-coated layer was dried at 100 °C, and the edge was removed with cotton. Then, it was annealed at 480 °C for 30 min with a slow heating ramp.

The PVSK precursor was made by mixing 0.461 g PbI_2 (99.99%, TCI) and 0.159 g CH_3NH_3I (Dyesol) in 73 μL of anhydrous dimethyl sulfoxide (DMSO, Aldrich) and 570 μL of anhydrous *N*,*N*-dimethylformamide (DMF, Aldrich). The precursor solution was spin-coated on the UV−O_3-treated TiO_2 mesoporous layer at 1200 rpm for 1 s and 2800 rpm for 25 s, and 300 μL of DEE was dripped at 14 s during the second spinning to form a transparent adduct. The film was transferred into an N_2-filled glovebox at <5% relative humidity and annealed at 60 °C for 10 min and 100 °C for 20 min.

Modification was achieved using thermally evaporated powder of MAI (Dyesol) in a low vacuum chamber with a base pressure of 1 × 10^{-2} Pa. As previously reported,[46,47] a precise calibration of MAI film is difficult to be obtained due to Volmer−Weber (island) growth characteristics onto flat substrates (e.g., glass or Si). The QCM was calibrated by evaporating different thickness of MAI onto silicon substrates and measuring the resultant thicknesses by profilometer (Figure S7).[47] Reported thicknesses of MAI evaporation are based on these nominal values measured with QCM.

The HTL precursor was prepared by mixing in chlorobenzene 70 mM of spiro (Merck), 231 mM *tert*-butylpiridine, 35 mM of bis(trifluoromethane) sulfonimide lithium salt (predissolved in acetonitrile) and 2.1 mM of tris(2-(1*H*-pyrazol-1-yl)-4-*tert*-butylpyridine)cobalt(III) tri[bis-(trifluoromethane)sulfonimide] (all additives and solvent from Aldrich). The spiro solution was deposited on the PVSK by dripping 30 μL of solution during spinning at 3000 rpm. Finally, 70 nm of gold was deposited as the top electrode by thermal evaporation.

J−*V* curves were measured the next day of fabrication to allow enough time for doping across the spiro film (Figures S8 and S9). The samples were stored in a low-humidity chamber overnight to enhance electrical properties of the HTL. *J*−*V* and steady-state measurements were performed under 1 sun illumination (AM 1.5 G, 100 mW·cm^{-2}, calibrated using a Newport reference Si-cell) using a solar simulator (Newport Oriel Sol 1A) and a Keithley 2400 source meter in ambient air at a relative humidity of ∼40−50% and using a 0.1 cm^2 mask. The measurements were done from −0.1 to 1.2 V in 40-point steps with a delay time of 10 ms.

ASSOCIATED CONTENT

Supporting Information

The Supporting Information is available free of charge on the ACS Publications website at DOI: 10.1021/acs.jpclett.7b01508.

Further UPS and XPS analysis and data, XRD and profilometer measurements, a discussion of current−voltage scans, and evolution of the photovoltaic parameters with MAI modifications. (PDF)

AUTHOR INFORMATION

Corresponding Authors

*Y.B.Q.: E-mail: Yabing.Qi@OIST.jp.
*N.-G.P.: E-mail: npark@skku.edu.

ORCID

Zafer Hawash: 0000-0001-9606-3521
Nam-Gyu Park: 0000-0003-2368-6300
Yabing Qi: 0000-0002-4876-8049

DOI: 10.1021/acs.jpclett.7b01508
J. Phys. Chem. Lett. 2017, 8, 3947−3953

Notes

The authors declare no competing financial interest.

■ ACKNOWLEDGMENTS

This work was supported by funding from the Energy Materials and Surface Sciences Unit of the Okinawa Institute of Science and Technology Graduate University, the OIST R&D Cluster Research Program, the OIST Proof of Concept (POC) Program, and JSPS KAKENHI Grant Number 15K17925. We thank Steven D. Aird, Technical Editor at Okinawa Institute of Science and Technology Graduate University, for improving the language of the manuscript. We thank Dr. Matthew R. Leyden for fabrication of automated multiple solar cells measurement system and Dr. Mikas Remeika for helping in writing part of the software for the system. D.-Y.S. and N.-G.P. are grateful to the National Research Foundation of Korea (NRF) and the Ministry of Science, ICT & Future Planning (MSIP) of Korea for financial support under contract nos. NRF-2012M3A6A7054861 (Global Frontier R&D Program on Center for Multiscale Energy System) and NRF-2015M1A2A2053004 (Climate Change Management Program).

■ REFERENCES

(1) Zhao, Y. X.; Zhu, K. Organic-inorganic hybrid lead halide perovskites for optoelectronic and electronic applications. *Chem. Soc. Rev.* **2016**, *45* (3), 655−689.

(2) Wang, Z.; Cheng, T.; Wang, F.; Dai, S.; Tan, Z. a. Morphology Engineering for High-Performance and Multicolored Perovskite Light-Emitting Diodes with Simple Device Structures. *Small* **2016**, *12* (32), 4412−4420.

(3) Yuan, M.; Quan, L. N.; Comin, R.; Walters, G.; Sabatini, R.; Voznyy, O.; Hoogland, S.; Zhao, Y.; Beauregard, E. M.; Kanjanaboos, P.; et al. Perovskite energy funnels for efficient light-emitting diodes. *Nat. Nanotechnol.* **2016**, *11* (10), 872.

(4) Lee, J. W.; Choi, Y. J.; Yang, J. M.; Ham, S.; Jeon, S. K.; Lee, J. Y.; Song, Y. H.; Ji, E. K.; Yoon, D. H.; Seo, S.; et al. In-Situ Formed Type I Nanocrystalline Perovskite Film for Highly Efficient Light-Emitting Diode. *ACS Nano* **2017**, *11* (3), 3311−3319.

(5) Chen, S.; Roh, K.; Lee, J.; Chong, W. K.; Lu, Y.; Mathews, N.; Sum, T. C.; Nurmikko, A. A Photonic Crystal Laser from Solution Based Organo-Lead Iodide Perovskite Thin Films. *ACS Nano* **2016**, *10* (4), 3959−3967.

(6) Zhu, H.; Fu, Y.; Meng, F.; Wu, X.; Gong, Z.; Ding, Q.; Gustafsson, M. V.; Trinh, M. T.; Jin, S.; Zhu, X. Lead halide perovskite nanowire lasers with low lasing thresholds and high quality factors. *Nat. Mater.* **2015**, *14* (6), 636−642.

(7) Xu, J.; Chen, Y.; Dai, L. Efficiently photo-charging lithium-ion battery by perovskite solar cell. *Nat. Commun.* **2015**, *6*, 8103.

(8) Luo, J.; Im, J.-H.; Mayer, M. T.; Schreier, M.; Nazeeruddin, M. K.; Park, N.-G.; Tilley, S. D.; Fan, H. J.; Graetzel, M. Water photolysis at 12.3% efficiency via perovskite photovoltaics and Earth-abundant catalysts. *Science* **2014**, *345* (6204), 1593−1596.

(9) Zhang, K.; Ma, M.; Li, P.; Wang, D. H.; Park, J. H. Water Splitting Progress in Tandem Devices: Moving Photolysis beyond Electrolysis. *Adv. Energy Mater.* **2016**, *6* (15), 1600602.

(10) Dou, L.; Yang, Y.; You, J.; Hong, Z.; Chang, W.-H.; Li, G.; Yang, Y. Solution-processed hybrid perovskite photodetectors with high detectivity. *Nat. Commun.* **2014**, *5*, 5404.

(11) Xiao, Z.; Yuan, Y.; Shao, Y.; Wang, Q.; Dong, Q.; Bi, C.; Sharma, P.; Gruverman, A.; Huang, J. Giant switchable photovoltaic effect in organometal trihalide perovskite devices. *Nat. Mater.* **2014**, *14* (2), 193−198.

(12) Xiao, Z.; Yuan, Y.; Wang, Q.; Shao, Y.; Bai, Y.; Deng, Y.; Dong, Q.; Hu, M.; Bi, C.; Huang, J. Thin-film semiconductor perspective of organometal trihalide perovskite materials for high-efficiency solar cells. *Mater. Sci. Eng., R* **2016**, *101*, 1−38.

(13) Park, N.-G. Perovskite solar cells: an emerging photovoltaic technology. *Mater. Today* **2015**, *18* (2), 65−72.

(14) Kim, H. S.; Lee, C. R.; Im, J. H.; Lee, K. B.; Moehl, T.; Marchioro, A.; Moon, S. J.; Humphry-Baker, R.; Yum, J. H.; Moser, J. E.; et al. Lead iodide perovskite sensitized all-solid-state submicron thin film mesoscopic solar cell with efficiency exceeding 9%. *Sci. Rep.* **2012**, *2*, 591.

(15) National Renewable Energy Laboratory (NREL). *Research Cell Efficiency Record*. http://www.nrel.gov/ncpv/images/efficiency_chart.jpg (accessed May 9, 2017).

(16) Ono, L. K.; Qi, Y. B. Surface and Interface Aspects of Organometal Halide Perovskite Materials and Solar Cells. *J. Phys. Chem. Lett.* **2016**, *7* (22), 4764−4794.

(17) Miller, E. M.; Zhao, Y.; Mercado, C. C.; Saha, S. K.; Luther, J. M.; Zhu, K.; Stevanovic, V.; Perkins, C. L.; van de Lagemaat, J. Substrate-controlled band positions in CH(3)NH(3)PbI(3) perovskite films. *Phys. Chem. Chem. Phys.* **2014**, *16* (40), 22122−22130.

(18) Olthof, S.; Meerholz, K. Substrate-dependent electronic structure and film formation of MAPbI3 perovskites. *Sci. Rep.* **2017**, *7*, 40267.

(19) Schulz, P.; Edri, E.; Kirmayer, S.; Hodes, G.; Cahen, D.; Kahn, A. Interface energetics in organo-metal halide perovskite-based photovoltaic cells. *Energy Environ. Sci.* **2014**, *7* (4), 1377.

(20) Li, L.; Liu, X. L.; Lyu, L.; Wu, R. S.; Liu, P.; Zhang, Y. H.; Zhao, Y.; Wang, H. Y.; Niu, D. M.; Yang, J. L.; et al. Modification of Ultrathin NPB Interlayer on the Electronic Structures of the CH3NH3PbI3/NPB/MoO3 Interface. *J. Phys. Chem. C* **2016**, *120* (32), 17863−17871.

(21) Olthof, S. Research Update: The electronic structure of hybrid perovskite layers and their energetic alignment in devices. *APL Mater.* **2016**, *4* (9), 091502.

(22) Wang, Q.; Shao, Y.; Xie, H.; Lyu, L.; Liu, X.; Gao, Y.; Huang, J. Qualifying composition dependent p and n self-doping in CH3NH3PbI3. *Appl. Phys. Lett.* **2014**, *105* (16), 163508.

(23) Emara, J.; Schnier, T.; Pourdavoud, N.; Riedl, T.; Meerholz, K.; Olthof, S. Impact of Film Stoichiometry on the Ionization Energy and Electronic Structure of CH3NH3PbI3 Perovskites. *Adv. Mater.* **2016**, *28* (3), 553−559.

(24) Cheng, Y.; Li, H.-W.; Zhang, J.; Yang, Q.-D.; Liu, T.; Guan, Z.; Qing, J.; Lee, C.-S.; Tsang, S.-W. Spectroscopic study on the impact of methylammonium iodide loading time on the electronic properties in perovskite thin films. *J. Mater. Chem. A* **2016**, *4* (2), 561−567.

(25) Son, D.-Y.; Lee, J.-W.; Choi, Y. J.; Jang, I.-H.; Lee, S.; Yoo, P. J.; Shin, H.; Ahn, N.; Choi, M.; Kim, D.; et al. Self-formed grain boundary healing layer for highly efficient CH3 NH3 PbI3 perovskite solar cells. *Nat. energy* **2016**, *1*, 16081.

(26) Cohen, B.-E.; Gamliel, S.; Etgar, L. Parameters influencing the deposition of methylammonium lead halide iodide in hole conductor free perovskite-based solar cells. *APL Mater.* **2014**, *2* (8), 081502.

(27) Roldan-Carmona, C.; Gratia, P.; Zimmermann, I.; Grancini, G.; Gao, P.; Graetzel, M.; Nazeeruddin, M. K. High efficiency methylammonium lead triiodide perovskite solar cells: the relevance of non-stoichiometric precursors. *Energy Environ. Sci.* **2015**, *8* (12), 3550−3556.

(28) Jacobsson, T. J.; Correa-Baena, J.-P.; Halvani Anaraki, E.; Philippe, B.; Stranks, S. D.; Bouduban, M. E. F.; Tress, W.; Schenk, K.; Teuscher, J.; Moser, J.-E.; et al. Unreacted PbI2 as a Double-Edged Sword for Enhancing the Performance of Perovskite Solar Cells. *J. Am. Chem. Soc.* **2016**, *138* (32), 10331−10343.

(29) Ahn, N.; Son, D. Y.; Jang, I. H.; Kang, S. M.; Choi, M.; Park, N. G. Highly Reproducible Perovskite Solar Cells with Average Efficiency of 18.3% and Best Efficiency of 19.7% Fabricated via Lewis Base Adduct of Lead(II) Iodide. *J. Am. Chem. Soc.* **2015**, *137* (27), 8696−8699.

(30) Lee, J. W.; Kim, H. S.; Park, N. G. Lewis Acid-Base Adduct Approach for High Efficiency Perovskite Solar Cells. *Acc. Chem. Res.* **2016**, *49* (2), 311−319.

DOI: 10.1021/acs.jpclett.7b01508
J. Phys. Chem. Lett. 2017, 8, 3947−3953

(31) Kim, T. G.; Seo, S. W.; Kwon, H.; Hahn, J.; Kim, J. W. Influence of halide precursor type and its composition on the electronic properties of vacuum deposited perovskite films. *Phys. Chem. Chem. Phys.* **2015**, *17* (37), 24342−24348.
(32) Endres, J.; Kulbak, M.; Zhao, L. F.; Rand, B. P.; Cahen, D.; Hodes, G.; Kahn, A. Electronic structure of the CsPbBr3/polytriarylamine (PTAA) system. *J. Appl. Phys.* **2017**, *121* (3), 035304.
(33) Liu, L.; McLeod, J. A.; Wang, R.; Shen, P.; Duhm, S. Tracking the formation of methylammonium lead triiodide perovskite. *Appl. Phys. Lett.* **2015**, *107* (6), 061904.
(34) Jung, M.-C.; Lee, Y. M.; Lee, H.-K.; Park, J.; Raga, S. R.; Ono, L. K.; Wang, S.; Leyden, M. R.; Yu, B. D.; Hong, S.; et al. The presence of CH3NH2 neutral species in organometal halide perovskite films. *Appl. Phys. Lett.* **2016**, *108* (7), 073901.
(35) Zhou, X.; Li, X.; Liu, Y.; Huang, F.; Zhong, D. Interface electronic properties of co-evaporated MAPbI3 on ZnO (0001): In situ X-ray photoelectron spectroscopy and ultraviolet photoelectron spectroscopy study. *Appl. Phys. Lett.* **2016**, *108* (12), 121601.
(36) Zou, Y.; Meng, Q.; Mao, H. Y.; Zhu, D. B. Substrate effect on the interfacial electronic structure of thermally-evaporated CH3NH3PbI3 perovskite layer. *Org. Electron.* **2017**, *41*, 307−314.
(37) Juarez-Perez, E. J.; Hawash, Z.; Raga, S. R.; Ono, L. K.; Qi, Y. B. Thermal degradation of CH3NH3PbI3 perovskite into NH3 and CH3I gases observed by coupled thermogravimetry-mass spectrometry analysis. *Energy Environ. Sci.* **2016**, *9* (11), 3406−3410.
(38) Leguy, A. M. A.; Hu, Y.; Campoy-Quiles, M.; Alonso, M. I.; Weber, O. J.; Azarhoosh, P.; van Schilfgaarde, M.; Weller, M. T.; Bein, T.; Nelson, J.; et al. Reversible Hydration of CH(3)NH(3)Pbl(3) in Films, Single Crystals, and Solar Cells. *Chem. Mater.* **2015**, *27* (9), 3397−3407.
(39) Song, Z. N.; Watthage, S. C.; Phillips, A. B.; Tompkins, B. L.; Ellingson, R. J.; Heben, M. J. Impact of Processing Temperature and Composition on the Formation of Methylammonium Lead Iodide Perovskites. *Chem. Mater.* **2015**, *27* (13), 4612−4619.
(40) Pellegrino, G.; Colella, S.; Deretzis, I.; Condorelli, G. G.; Smecca, E.; Gigli, G.; La Magna, A.; Alberti, A. Texture of MAPbI3 layers assisted by chloride on flat TiO2 substrates. *J. Phys. Chem. C* **2015**, *119*, 19808.
(41) Da, P.; Zheng, G. Tailoring interface of lead-halide perovskite solar cells. *Nano Res.* **2017**, *10*, 1471.
(42) Jung, M. C.; Raga, S. R.; Ono, L. K.; Qi, Y. B. Substantial improvement of perovskite solar cells stability by pinhole-free hole transport layer with doping engineering. *Sci. Rep.* **2015**, *5*, 9863.
(43) Hawash, Z.; Ono, L. K.; Qi, Y. B. Moisture and Oxygen Enhance Conductivity of LiTFSI-Doped Spiro-MeOTAD Hole Transport Layer in Perovskite Solar Cells. *Adv. Mater. Interfaces* **2016**, *3* (13), 1600117.
(44) Hawash, Z.; Ono, L. K.; Raga, S. R.; Lee, M. V.; Qi, Y. B. Air-Exposure Induced Dopant Redistribution and Energy Level Shifts in Spin-Coated Spiro-MeOTAD Films. *Chem. Mater.* **2015**, *27* (2), 562−569.
(45) Perkins, C. L.; Hasoon, F. S. Surfactant-assisted growth of CdS thin films for photovoltaic applications. *J. Vac. Sci. Technol., A* **2006**, *24* (3), 497−504.
(46) Malinkiewicz, O.; Yella, A.; Lee, Y. H.; Minguez Espallargas, G.; Graetzel, M.; Nazeeruddin, M. K.; Bolink, H. J. Perovskite solar cells employing organic charge-transport layers. *Nat. Photonics* **2013**, *8* (2), 128−132.
(47) Ono, L. K.; Wang, S.; Kato, Y.; Raga, S. R.; Qi, Y. B. Fabrication of semi-transparent perovskite films with centimeter-scale superior uniformity by the hybrid deposition method. *Energy Environ. Sci.* **2014**, *7*, 3989.

DOI: 10.1021/acs.jpclett.7b01508
J. Phys. Chem. Lett. 2017, 8, 3947−3953